https://doi.org/10.5194/egusphere-2026-5795
Preprint. Discussion started: 11 November 2026
© Author(s) 2026. CC BY 4.0 License.

Evaluating Oxidant Field Representations in Aerosol Modeling: Insights from the ASIA-AQ Campaign and Global Budgets

Huisheng Bian[1,2], Patricia Castellanos[2], Allison Collow[1,2], Ravi C. Govindaraju[3,2], Pamela A. Wales[4,2], Ryan Boyd[5], John Crounse[6], Arlindo M Da Silva[7,8], Mark A. Zondlo[5], Eric Apel[9], Katherine Ball[6], Yunseo Choi[5], Jose-Luis Jimenez[10], Richard H. Moore[11], and James H. Crawford[11]

[1]Goddard Earth Sciences Technology and Research (GESTAR) II, University of Maryland Baltimore County, Baltimore, MD, USA.

[2]NASA Goddard Space Flight Center, Greenbelt, MD, USA.

[3]Science Systems and Applications Inc., MD, USA

[4]Morgan State University, MD, USA.

[5]Department of Civil and Environmental Engineering, Princeton University, NJ, USA.

[6]Division of Geological and Planetary Sciences, California Institute of Technology (Caltech), CA, USA.

[7]Center for Research on Sustainable Forests, University of Maine, Orono, ME, USA

[8]Asticou Earth Systems LLC, Bar Harbor, Maine, USA

[9]Atmospheric Chemistry Observations and Modeling Laboratory, National Center for Atmospheric Research (NCAR), CO, USA.

[10]Cooperative Institute for Research in Environmental Sciences (CIRES) and Department of Chemistry, University of Colorado Boulder, CO, USA.

[11]NASA Langley Research Center, Hampton, VA, USA.

Correspondence to: Huisheng Bian (huisheng.bian@nasa.gov)

Abstract

Accurate prediction of secondary inorganic aerosols (e.g., sulfate and nitrate) relies heavily on representing highly variable, nonlinear atmospheric oxidant chemistry. This study systematically evaluates the sensitivity of the Goddard Chemistry, Aerosol, Radiation, and Transport second-generation (GOCART-2G) aerosol simulations to prescribed OH, H_2O_2, and NO_3 radical oxidants and the nitrate precursor HNO_3. Specifically, we compare three GOCART-2G simulations: using hourly GEOS Composition Forecast (GEOS-CF) fields generated using GEOS-Chem, using monthly means of the same fields, and using MERRA2-GMI monthly climatology. Model performance was assessed using airborne data from the 2024 ASIA-AQ campaign (covering the Philippines, South Korea, and Thailand). A separate annual global sensitivity analysis examines sulfur and nitrate budgets for 2019. Compared to simulation using monthly GEOS-CF data, simulation using hourly data improves the correlations between the modeled results (oxidant, sulfate, and nitrate) and airborne observational data. Capturing hourly-term variability—particularly the strong diurnal cycles of OH and NO_3—preserves the temporal covariance and nonlinear coupling that monthly means obscure. Consequently, hourly-resolved oxidants weaken the overall chemical transformation of dimethyl sulfide (DMS). This results in more than 20% higher global DMS and methanesulfonic acid (MSA) burdens than monthly mean simulations,

https://doi.org/10.5194/egusphere-2026-5795
Preprint. Discussion started: 11 November 2026
© Author(s) 2026. CC BY 4.0 License.



while exerting substantial regional impacts (>20%) on sulfur and nitrate budgets over East Asia. Simulation results based on MERRA2-GMI and GEOS-CF monthly data show discrepancies in sulfate and nitrate loadings, reflecting differences in the prescribed-field configurations used in the two datasets. These findings highlight the limitations of decoupled, time-averaged oxidant fields in traditional global models, demonstrating that resolving high-frequency temporal variability and nonlinear feedbacks is critical for Earth System Models.

1. Introduction

Atmospheric aerosols play a critical role in the Earth system by scattering and absorbing solar radiation (Bellouin et al., 2020), modifying cloud microphysical properties (Forster et al., 2021), and influencing weather (Zhang et al., 2022), air quality (Fuzzi et al., 2015), and climate (Forster et al., 2021). Global aerosol models therefore simulate the emission, transport, chemical transformation, and removal of atmospheric particles and have become an integral component of modern weather and climate prediction systems. Among the processes governing aerosol evolution, the formation of secondary inorganic aerosols, particularly sulfate and nitrate, depends strongly on atmospheric oxidant chemistry. It has long been recognized that accurately representing oxidant chemistry is essential for predicting secondary aerosol production because oxidant concentrations exhibit strong temporal variability and participate in highly nonlinear chemical interactions with aerosol precursors and aerosols (Aw and Kleeman, 2003; Zheng et al., 2015; Paulot et al., 2017; Valin et al., 2011).

The concentrations of key oxidants, including OH, O_3, H_2O_2, and NO_3, can vary substantially on hourly to synoptic timescales in response to changes in emissions, meteorology, cloud processing, and boundary layer dynamics. These transient conditions often account for a disproportionate fraction of total secondary aerosol production (Jacob, 2000; Seinfeld and Pandis, 2016; Brown and Stutz, 2012; Carlton et al., 2018; Ervens, 2015). The underlying chemistry is highly nonlinear. Gas-phase production of OH and O_3 depends nonlinearly on NO_x ($NO + NO_2$) and volatile organic compound (VOC) concentrations, thereby strongly influencing sulfate and nitrate formation. Sulfate production through aqueous-phase oxidation by H_2O_2 or O_3 further depends on cloud liquid water content, aerosol pH, and oxidant availability (Alexander et al., 2005; Pye et al., 2020), while nighttime NO_3 chemistry can substantially enhance nitrate production under favorable conditions (Brown and Stutz, 2012). Aerosols also modify oxidant abundances through radiative effects that alter photolysis rates and through heterogeneous chemical reactions occurring on particle surfaces (Jacobson, 2001; Tie et al., 2005), introducing additional feedbacks between atmospheric chemistry and aerosol evolution.

Despite the importance of these interactions, explicitly simulating atmospheric chemistry remains computationally demanding because it requires solving the coupled transport and chemical evolution of hundreds of reactive species across a wide range of spatial and temporal scales. Consequently, many global aerosol models employ simplified aerosol chemistry parameterizations that retain the dominant processes while reducing computational cost. One

https://doi.org/10.5194/egusphere-2026-5795
Preprint. Discussion started: 11 November 2026
© Author(s) 2026. CC BY 4.0 License.

such scheme is the Goddard Chemistry, Aerosol, Radiation, and Transport second-generation (GOCART-2G) aerosol model (Chin et al., 2002; Colarco et al., 2010; Collow et al., 2024). Second-generation (2G) refers to a recent modernization of the legacy GOCART codebase and scientific enhancements. GOCART-2G is implemented in the Goddard Earth Observing System (GEOS) model to enable multidecadal aerosol reanalysis and aerosol forecasts on short term through subseasonal-to-seasonal timescales. The GEOS Forward Processing (GEOS-FP) system is designed for near-real time numerical weather prediction including radiatively interactive aerosols that are constrained by assimilation of aerosol optical depth.

To achieve computational efficiency for systems such as GEOS-FP, GOCART-2G is commonly operated within GEOS in a configuration that is decoupled from explicit gas-phase chemistry. Instead of predicting oxidants interactively, secondary aerosol formation is driven using prescribed oxidant fields, including OH, O_3, H_2O_2, NO_3, and HNO_3, derived from comprehensive chemistry simulations. Similar approaches are widely employed in global aerosol models (Mann et al., 2010; Zhang et al., 2012). This design choice, reducing computational expense while maintaining realistic large-scale aerosol distributions, is intentional for three main reasons. First, computational efficiency is essential for time-sensitive applications such as near–real-time support for aircraft field campaigns. Second, computational efficiency is also essential for multi-decadal simulations in Earth System Models (ESM). Third, it provides a controlled framework for isolating aerosol physical and chemical processes without the added computational expense and complexity of fully coupled chemistry.

However, prescribed oxidant fields cannot respond dynamically to changing emissions, meteorology, or chemical environments and therefore cannot fully capture the temporal variability and nonlinear chemical feedbacks that govern secondary aerosol formation. Our preliminary study indicated notable differences between GOCART simulations driven by prescribed monthly oxidant fields and those coupled to full gas-phase chemistry, particularly over East Asia, where secondary inorganic aerosol formation is highly sensitive to oxidant availability. Although GOCART-2G has evolved considerably since its original development for satellite aerosol applications, prescribed oxidant fields remain the default treatment in many GEOS aerosol products, including the Modern-Era Retrospective Analysis for Research and Applications, Version 2 (MERRA-2) aerosol reanalysis (Randles et al., 2017), one of the most widely used global aerosol datasets in the atmospheric science community. These findings, together with the widespread use of the uncoupled GOCART configuration, motivate a systematic evaluation of how different representations of oxidant fields influence aerosol simulations.

In this study, we investigate the sensitivity of GOCART-2G aerosol simulations to different representations of atmospheric oxidants. Specifically, we compare simulations driven by three oxidant field implementations to examine (1) how the temporal representation of oxidants influences secondary aerosol formation when the underlying chemical mechanism is held fixed, and (2) how aerosol simulations respond to oxidant fields generated by different chemical

https://doi.org/10.5194/egusphere-2026-5795
Preprint. Discussion started: 11 November 2026
© Author(s) 2026. CC BY 4.0 License.

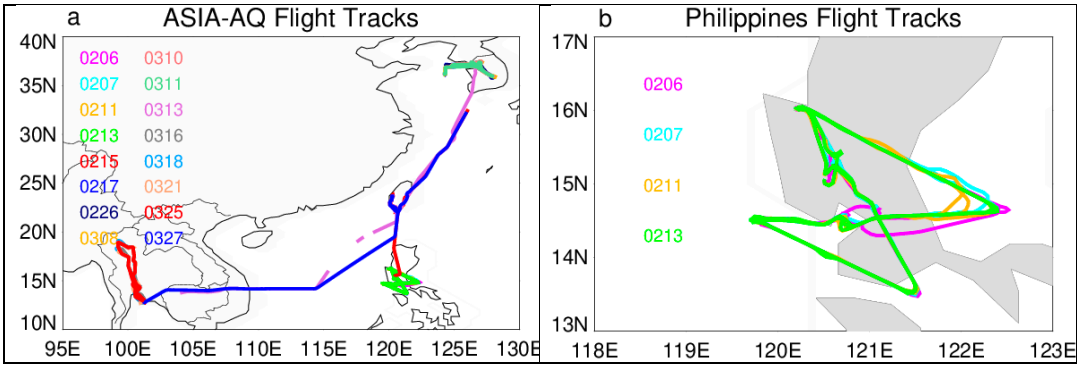
mechanisms. The analysis is conducted during the Airborne and Satellite Investigation of Asian Air Quality (ASIA-AQ) field campaign, which provides an exceptional observational dataset for evaluating model performance. Conducted during February and March 2024 over the Philippines, South Korea, and Thailand, ASIA-AQ collected comprehensive airborne measurements of sulfate, nitrate, and key precursor species including DMS, SO_2, HNO_3, NH_3, OH, and H_2O_2 across chemically diverse environments ranging from relatively clean marine regions to highly industrialized urban areas and biomass-burning-influenced regions.

The remainder of this paper is organized as follows. Section 2 describes the ASIA-AQ observations, the NASA GEOS Earth System Model and its aerosol and chemistry components, and the experimental design. Section 3 presents the model evaluation and sensitivity analyses, beginning with comparisons against ASIA-AQ observations and subsequently extending the analysis to global simulations to investigate the influence of oxidant temporal variability and chemical mechanism on aerosol formation. Section 4 summarizes the principal findings and discusses their implications for global aerosol modeling.

2. Data, model, and experiments

2.1 ASIA-AQ measurements

The Airborne and Satellite Investigation of Asian Air Quality (ASIA-AQ) is an aircraft campaign conducted across Asia during February–March 2024, primarily over three countries: Philippines, South Korea, and Thailand (Crawford et al., 2022). NASA deployed the DC-8 aircraft for 16 research flights across these targeted countries. The DC-8 flight times and flight tracks are shown in Fig. 1. ASIA-AQ aimed to deepen understanding of the factors influencing local air quality across Asia by integrating diverse observational approaches with advanced modeling techniques (https://espo.nasa.gov/asia-aq). Table 1 summarizes the measured aerosol properties, associated gas-phase precursors and oxidant fields, and the instruments onboard the DC-8 used in this study. These in situ measurements encompass the major aerosol components for these areas as well as relevant gas precursors and oxidants, thereby providing robust and comprehensive constraints for interpreting observations and improving aerosol representations in models.



https://doi.org/10.5194/egusphere-2026-5795
Preprint. Discussion started: 11 November 2026
© Author(s) 2026. CC BY 4.0 License.

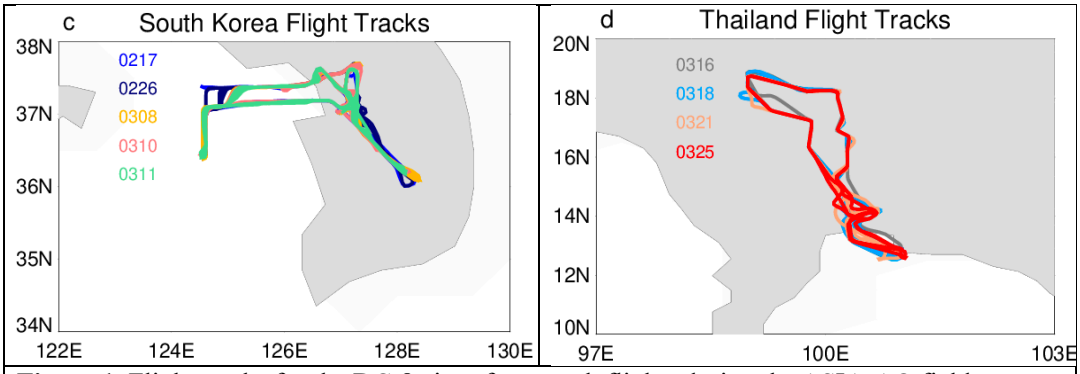


Figure 1. Flight tracks for the DC-8 aircraft research flights during the ASIA-AQ field mission.

Table 1: AISA-AQ DC-8 measurement aerosol-related species used in this study

Quantity name	Description	Data version	Instrument	Primary Investigator
BC_mass	In situ accumulation-mode black carbon aerosol at STP	R1	SP2	Richard Moore
OA_PM1.5_AMS_60s	Mass concentration of PM1 organic aerosol in air at STP	R1, R2	AMS	Jose-Luis Jimenez
Sulfate_PM1.5_AMS_60s	Mass concentration of PM1 sulfate aerosol in air at STP	R1, R2	AMS	Jose-Luis Jimenez
Nitrate_PM1.5_AMS_60s	Mass concentration of PM1 nitrate aerosol in air at STP	R1, R2	AMS	Jose-Luis Jimenez
Ammonium_PM1.5_AMS_60s	Mass concentration of PM1 ammonium aerosol in air at STP	R1, R2	AMS	Jose-Luis Jimenez
MSA_PM1.5_AMS_60s	Mass concentration of PM1 MSA aerosol in air at STP	R1, R2	AMS	Jose-Luis Jimenez
Seasalt_PM1.5_AMS_60s	Mass concentration of PM1 sea salt aerosol in air at STP	R1, R2	AMS	Jose-Luis Jimenez
StdtoVol_PM1.5_AMS_60s	Conversion factor from std to ambient volume and pressure	R1, R2	AMS	Jose-Luis Jimenez
DMS_TOGA	In situ gas DMS	R1	TOGA	Eric Apel
SO2_CIT	Volume mixing ratio of sulfur dioxide in air	R0, R1	CIT-HToF-CIMS	Paul Wennberg
H2O2_CIT	Volume mixing ratio of hydrogen peroxide in air	R0	CIT-HToF-CIMS	Paul Wennberg
HNO3_CIT	Volume mixing ratio of nitric acid in air	R0	CIT-HToF-CIMS	Paul Wennberg
NH3	Volume mixing ratio of ammonia in air	R2	OPALS	Mark Zondlo

AMS: Aerosol Mass Spectrometer
CIT-HToF-CIMS: Chemical Ionization High Resolution Time of Flight Mass Spectrometer
OPALS: Open-Path Ammonia Laser Spectrometer
SP2: a Single Particle Soot Photometer
STP: standard Temperature and Pressure
TOGA: NCAR Trace Organic Gas Analyzer

Table 1. Measurements of aerosol-related species made onboard the DC-8 during ASIA-AQ that were used in this study. Please note that there are two versions of both the AMS and the CIT-HToF-CIMS, as the version numbers vary depending on the date.

145

In the aircraft observation-model comparisons, we used 60 second merged observations (https://www-air.larc.nasa.gov/missions/etc/onlinemergedoc.pdf). The model was sampled at the time and location of the aircraft from the time averaged observation files. For aerosol related

https://doi.org/10.5194/egusphere-2026-5795
Preprint. Discussion started: 11 November 2026
© Author(s) 2026. CC BY 4.0 License.

measurements, such as the Aerosol Mass Spectrometer (AMS), we calculated the GEOS-simulated aerosol mass that matches the observed particle size range specific to the instrument.

2.2 **GEOS model description**

NASA GEOS is a modular Earth system model that integrates atmospheric dynamics, physics, and chemistry. GEOS GEOS-FP provides weather and bulk aerosol analyses and forecasts, whereas GEOS Composition Forecast (GEOS-CF) predicts atmospheric composition using online GEOS-Chem chemistry (Long et al., 2015). GEOS also supports the Global Modeling Initiative (GMI) chemical mechanism (Strahan et al., 2007). GOCART-2G in GEOS-FP is the aerosol module used in the simulations examined here; it treats aerosol processes and simplified secondary aerosol formation without a comprehensive gas-phase chemical solver (Chin et al., 1996, 2002; Colarco et al., 2010; Collow et al., 2024). CFH (using hourly GEOS-CF data), CFM (using monthly GEOS-CF data), and GMI (using monthly MERRA2-GMI data) (see details in section 3.2) denote three prescribed-oxidant-field simulations by GOCART-2G, not three distinct aerosol models. The GEOS simulations in this study are operated in replay mode (Orbe et al., 2017), with meteorology constrained by archived GEOS for Instrument Teams (GEOS-IT) analyses (https://gmao.gsfc.nasa.gov/gmao-products/geos-it/). In other words, the temperature, humidity, and wind fields are constrained to the analysis from GEOS-IT with a corrector step every 6 hours. Simulations for this study are conducted at a global horizontal resolution of approximately 25 km with 72 vertical sigma levels extending from the surface to 0.01 hPa (~85 km).

GOCART-2G simulates major atmospheric aerosol species and their precursors, including sulfate (SO_4), nitrate (NO_3), ammonium (NH_4), black carbon (BC), organic aerosol (OA), brown carbon (BR), dust, sea salt, particulate methanesulfonate (MSA), dimethyl sulfide (DMS), sulfur dioxide (SO_2), and ammonia (NH_3) (Bian et al., 2017, 2019, 2024; Chin et al., 2009, 2014; Colarco et al., 2010; Collow et al., 2024). Sulfate and nitrate are treated as secondary aerosols formed from precursor gases emitted by anthropogenic, biomass-burning, oceanic, and volcanic sources (SO_2 only). MSA is produced through the oxidation of DMS. Detailed description of carbonaceous aerosols (e.g., BC, OA, and BR) is given in the Supplementary Material.

Natural emissions of dust, sea salt, and DMS are calculated online based on simulated near-surface winds and surface properties. Specifically, DMS emissions are estimated using monthly climatological DMS concentrations in seawater from Lana et al. (2011), together with modeled sea surface temperature and 10-meter wind speed. The wind speed dependence follows the parameterization of Liss and Merlivat (1986). Most aerosol species are represented in the fine mode, while nitrate, dust, and sea salt also include coarse-mode bins. Dust and sea salt are both modeled by five non-interacting size bins, while nitrate is modeled with three size bins. Details of aerosol size information can be found in Collow et al. (2024). For the 2019 simulations, anthropogenic emissions are prescribed monthly from the Community Emission Data System

https://doi.org/10.5194/egusphere-2026-5795
Preprint. Discussion started: 11 November 2026
© Author(s) 2026. CC BY 4.0 License.

2019 record (CEDS; Hoesly et al., 2018), spanning nine sectors: energy, industry, road transportation, residential, waste, agriculture, solvent use, shipping, and aviation. Emissions from all sectors are released at the surface, except for those from the energy and aviation sectors, which are distributed vertically. The 2024 simulations reuse the same 2019 monthly anthropogenic emissions because the CEDS v2021_v04 inventory used here ends in 2019. Both study periods use contemporaneous daily biomass-burning emissions of OA, BC, SO_2 and NH_3 from version 2.6r1 of the Quick Fire Emission Dataset (QFED; Darmenov and da Silva, 2015). Volcanic SO_2 emissions, including both degassing and eruptive sources, are derived from OMI satellite observations (Carn et al., 2017).

The prescribed chemical fields used here comprise the oxidants OH, H_2O_2, and NO_3 radical and the nitrate precursor HNO_3; collectively, these are denoted OX. HNO_3 is distinguished from the oxidants throughout. O_3 contributes to sulfur chemistry generally but is not used directly by the GOCART-2G sulfate chemistry evaluated here. In the default GEOS-FP approach, OX is obtained from MERRA2-GMI, a retrospective chemistry simulation using the GMI mechanism and MERRA-2 meteorology (Strahan et al., 2007; Gelaro et al., 2017; Strode et al., 2019; https://acd-ext.gsfc.nasa.gov/Projects/GEOSCCM/MERRA2GMI/). Output is archived on the native MERRA-2 grid (0.625° longitude × 0.5° latitude). GOCART is interactively coupled in the source simulation, but feedback of nitrate aerosol formation on gas-phase HNO_3 is not included. A uniform global scaling factor is applied to the MERRA2-GMI HNO_3 fields used by the GMI experiment to compensate for the missing HNO_3 sink associated with nitrate aerosol formation and to improve lower-tropospheric HNO_3. GEOS-FP uses year-specific monthly mean OX fields through 2018 and a 1980–2018 monthly climatology thereafter. Consequently, the GMI experiment uses this climatology for both 2019 and 2024.

As GOCART-2G is agnostic to the chemical mechanism producing the OX fields, other offline chemical simulations can also be utilized. A contemporaneous forecasting system to GEOS-FP is the GEOS Composition Forecast (GEOS-CF). This system is designed for predicting detailed atmospheric chemistry and aerosol processes by integrating the GEOS-Chem chemical module into the GEOS ESM (Hu et al., 2018; Keller et al., 2021). Since Keller et al. (2021), the version 2 update of the GEOS-CF system includes updating to GEOS-Chem version 14.0.0 and monthly anthropogenic emissions to the CEDS 2019 record (v2021_v04: O'Rourke et al., 2021). The GEOS-Chem mechanism includes coupled nitrate aerosol and trace gas chemistry with secondary inorganic aerosols recently evaluated by Norman et al. (2025), so no analogous additional HNO_3 scaling is applied to CFH or CFM. This difference in HNO_3 treatment is part of the GMI–CFM comparison and must not be attributed solely to the gas-phase chemical mechanism. Relevant updates to the v14.0.0 mechanism since Keller et al. (2021) include updated cloud-water pH and aerosol uptake coefficients for NO_2, NO_3, and N_2O_5 (Holmes et al., 2019; McDuffie et al., 2018; Shah et al., 2020).

https://doi.org/10.5194/egusphere-2026-5795
Preprint. Discussion started: 11 November 2026
© Author(s) 2026. CC BY 4.0 License.

The GEOS-CF (v2) system produces daily a 1-day hindcast and a 5-day forecast of global atmospheric composition with the hindcast segment replaying to the GEOS for Instrument Teams (GEOS-IT) meteorological analysis and assimilating satellite-based observations of ozone. As the GEOS-CF simulation would respond to dynamic emission events (such as biomass burning) and meteorology similar to GEOS-FP, it would be advantageous to use the higher temporal fidelity of the GEOS-CF forecasts to drive the GOCART-2G secondary aerosol formation in GEOS-FP, thereby establishing a one-way coupling configuration between GEOS-FP and GEOS-CF. In the following, we describe two modeling experiments to evaluate the impact of using GEOS-CF offline predicted OX fields to drive GOCART-2G, with performance evaluated against aircraft observations from the ASIA-AQ field experiment.

2.3 Experiment design

We conducted a set of GOCART-2G simulations using OX fields derived from GEOS-CF in two different ways. First, we performed a replay simulation of GEOS-CF (v2) for the time periods of interest at c360 cubed-sphere horizontal resolution and archived the GEOS-CF predicted oxidant oxidant fields at 0.25° × 0.25° horizontal and 1-hourly resolution and used these time-varying OX to drive the GOCART-2G aerosol simulation. We refer to this configuration as CFH. A second simulation was then conducted using monthly mean OX derived from the GEOS-CF hourly dataset. This configuration, referred to as CFM, is analogous to GMI which uses OX from the MERRA2-GMI monthly climatology currently utilized by GOCART-2G. Thus, by comparing the CFM and GMI simulations we can first isolate differences in different sources of the simulated OX fields, while comparing the CFM and CFH simulations isolates the impact of including higher fidelity temporal variability in the OX fields.

All three experiments were conducted for February–March 2024 to evaluate model performance during ASIA-AQ and for 2019 to assess annual global sensitivity; 2019 is the final year covered by the anthropogenic emission inventory used here. The GOCART-2G simulations share identical meteorology, emissions, resolution, and aerosol processes, differing only in their prescribed OX fields. However, the GEOS-CF and MERRA2-GMI source simulations differ in chemical mechanism, meteorology (GEOS-IT versus MERRA-2), averaging period, resolution, emissions, and HNO_3 treatment. The GMI–CFM comparison therefore reflects these combined source differences and cannot isolate the chemical mechanism alone. The three simulations using the three described strategies for oxidant fields are summarized in Table 2. Note the archived-field averaging interval and the GOCART-2G application interval are distinct.

Table 2. The designed model experiments with three oxidant fields.

Experiment Name	Chemical Mechanism	Temporal Resolution[1]	Update (minutes)[2]	Purpose
GMI	GMI-Chem	Monthly	180	Default oxidant configuration

https://doi.org/10.5194/egusphere-2026-5795
Preprint. Discussion started: 11 November 2026
© Author(s) 2026. CC BY 4.0 License.

CFM	GEOS-Chem	Monthly	180	Assess the impact of chemical representation comparing CFM to GMI
CFH	GEOS-Chem	Hourly	12.5	Assess the impact of oxidants temporal variation comparing CFH and CFM

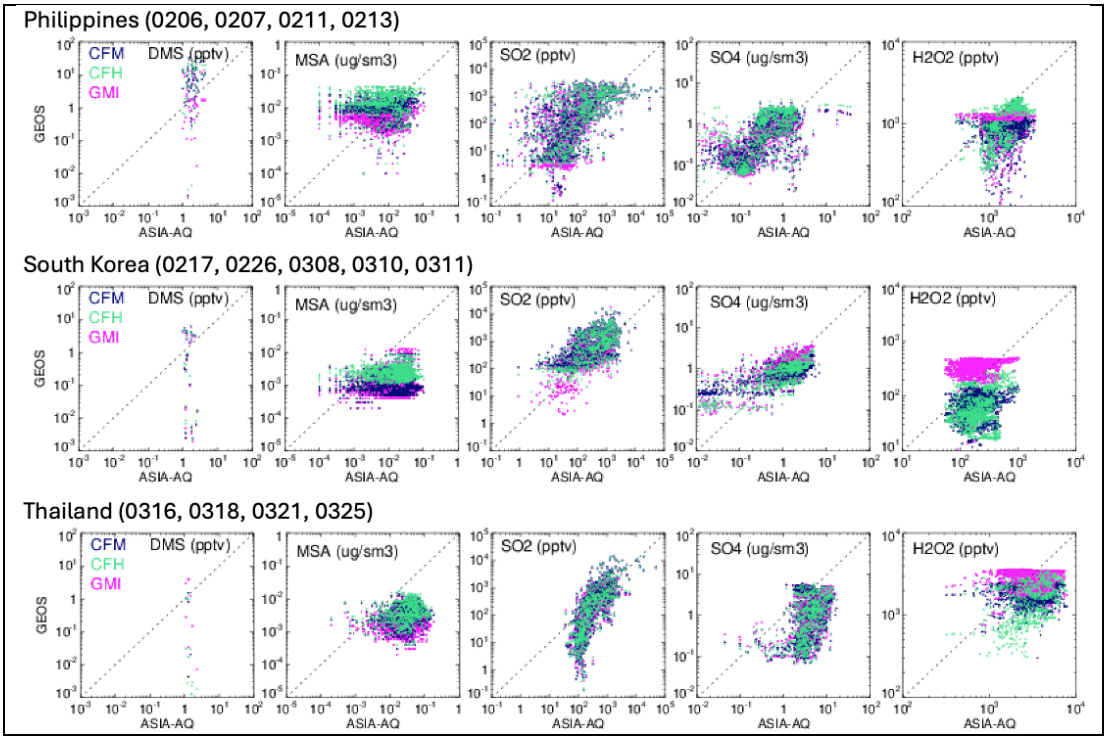
[1]Time interval over which the archived oxidant fields are averaged.
[2]Time interval at which GOCART-2G updates the oxidant fields.

3. Results

3.1 Analysis over ASIA-AQ locations and time period

3.1.1 Evaluation during ASIA-AQ field campaign

Results presented here are for the sulfate and nitrate families, as these species are most sensitive to chemical reactions within the simplified parameterization of GOCART-2G. To understand the reasons for the simulated aerosol differences, we also analyzed the corresponding oxidant fields (i.e., OH, NO_3, H_2O_2, and HNO_3). Figure 2 presents a comparison of scatter plots showing concentrations of sulfate-related species derived from GEOS simulations against field observations from the ASIA-AQ campaign over the three distinct domains (Philippines, South Korea, and Thailand). Figure 3 displays similar comparative results for nitrate-related species. The corresponding correlation coefficients and ratios of mean tracer concentrations between GEOS simulation results and ASIA-AQ measurements are given in Tables 3 and 4, respectively.



https://doi.org/10.5194/egusphere-2026-5795
Preprint. Discussion started: 11 November 2026
© Author(s) 2026. CC BY 4.0 License.

Figure 2. Scatter plots comparing concentrations of sulfate species from three GEOS simulations to ASIA-AQ measurements for the flights over the Philippines (top panel), South Korea (middle panel), and Thailand (bottom panel). The corresponding correlation coefficients and ratios of mean tracer concentrations between GEOS simulation results and ASIA-AQ measurements are given in Table 3.

Table 3. Correlation coefficients (R) and ratios of mean concentrations between model and observation for sulfate-related species during ASIA-AQ (Fig. 2).

		DMS		MSA		SO_2		SO_4		H_2O_2	
		R	Ratio	R	Ratio	R	Ratio	R	Ratio	R	Ratio
Philippines	CFH	0.44	5.58	0.11	1.15	0.11	0.58	0.35	1.16	0.50	0.65
	CFM	0.27	4.58	0.16	0.85	0.12	0.56	0.32	1.06	0.10	0.53
	GMI	0.09	2.62	0.12	0.51	0.11	0.58	0.33	0.98	0.04	0.61
South Korea	CFH	0.10	1.11	0.04	0.12	0.37	1.49	0.57	0.62	0.40	0.32
	CFM	0.09	1.13	0.09	0.05	0.36	1.59	0.51	0.57	0.30	0.29
	GMI	0.09	1.01	0.12	0.07	0.35	1.41	0.56	0.77	0.22	1.55
Thailand	CFH	0.16	0.09	0.14	0.10	0.43	0.96	0.29	0.33	0.32	0.87
	CFM	0.16	0.09	0.12	0.09	0.44	1.00	0.19	0.33	0.05	0.58
	GMI	0.15	0.32	0.11	0.06	0.43	0.95	0.29	0.34	0.13	0.85

Beyond the primary aerosol families, the evaluation reveals distinct model-measurement discrepancies for key precursor species, specifically DMS and NH_3. Although these precursor variations are explored in greater detail below, their initial structural divergence from observations underpins the broader correlation and bias trends discussed herein. Overall, the hourly oxidant field (CFH) approach significantly improved the correlation between the simulated and observed oxidant fields (e.g., H_2O_2 and HNO_3). Consequently, the sulfate and nitrate species simulated using the CFH OX fields demonstrated a slightly better correlation with the observational data. Here, we emphasize correlation rather than absolute differences, as correlation serves as a more accurate reflection of the dynamics of the fundamental physical and chemical processes embedded within the model, whereas absolute differences can often be artificially adjusted by tuning emission input data or loss efficiency. These results underscore the necessity for further research into precursor species—specifically DMS and NH_3—which have historically received less attention than sulfate and nitrate aerosols. As noted by Bian et al. (2017), uncertainties regarding precursor emissions and oxidation pathways remain one of the primary limitations facing global models in the simulation of secondary inorganic aerosols.

In analyzing these specific precursor discrepancies, simulated DMS concentrations during the ASIA-AQ campaign over the Philippines domain— a region influenced by both local anthropogenic emissions from the islands and marine emissions from the surrounding open ocean—were consistently overestimated by all three modeling approaches, with biases ranging from a factor of 2 to 6. In contrast, simulations for the Korean Peninsula region were generally comparable to observed values, whereas simulations for the inland region of Thailand showed severe underestimation (ranging from only one-tenth to one-third of the observed DMS values).

https://doi.org/10.5194/egusphere-2026-5795
Preprint. Discussion started: 11 November 2026
© Author(s) 2026. CC BY 4.0 License.

DMS correlations are weak over South Korea and Thailand (R = 0.09–0.16) and vary more widely over the Philippines (R = 0.09–0.44), where CFH has the highest correlation. Table 3 also shows that the ratio of the mean DMS concentrations between model and observation varies by location, showing no consistent improvement relative to the observed data. This poor performance in simulating DMS partially explains the biases and low correlation in the simulated concentrations of MSA; interestingly, however, the simulated concentrations of SO_2 and SO_4 do not appear to have been significantly impacted by these substantial biases in DMS simulation as this sulfate formation pathway of DMS is relatively minor in polluted regions.

Parallel to the DMS variations, the GEOS model consistently simulated NH_3 concentrations that were significantly lower than the observed values, regardless of the specific oxidant field used. This systemic underestimation suggests that the most probable explanation for this discrepancy is that, across all simulation experiments, the NH_3 emission estimates provided by the CEDS emission inventory for the aforementioned regions and seasons were systematically too low. A recent multi-model intercomparison effort over Korea during the ASIA-AQ time period also revealed a systematic low bias in NH_3 by all but one model (Jeong et al., 2026). The fifteen models considered in the study contained various levels of complexity with regards to atmospheric chemistry, and yet all still displayed a similar degree of low bias, strongly indicating an underestimation in NH_3 sources. However, other potential causes, such as the simplified aerosol chemical mechanism used in GOCART-2G cannot be ruled out.

Although no single simulation consistently provides the best agreement with observations across all species and regions, these comparisons demonstrate that the temporal representation of oxidants affects chemically coupled species in a strongly species- and region-dependent manner. In particular, changes in oxidant fields do not translate proportionally into changes in their reaction products, suggesting that the effects of temporal averaging extend beyond simply smoothing short-term oxidant variability. These results motivate the analysis in Section 3.2, where we examine how the use of monthly mean versus hourly oxidant fields alters the temporal covariance and nonlinear coupling among reactants and products, and consequently affects sulfur and nitrate budgets at regional and global scales.

https://doi.org/10.5194/egusphere-2026-5795
Preprint. Discussion started: 11 November 2026
© Author(s) 2026. CC BY 4.0 License.

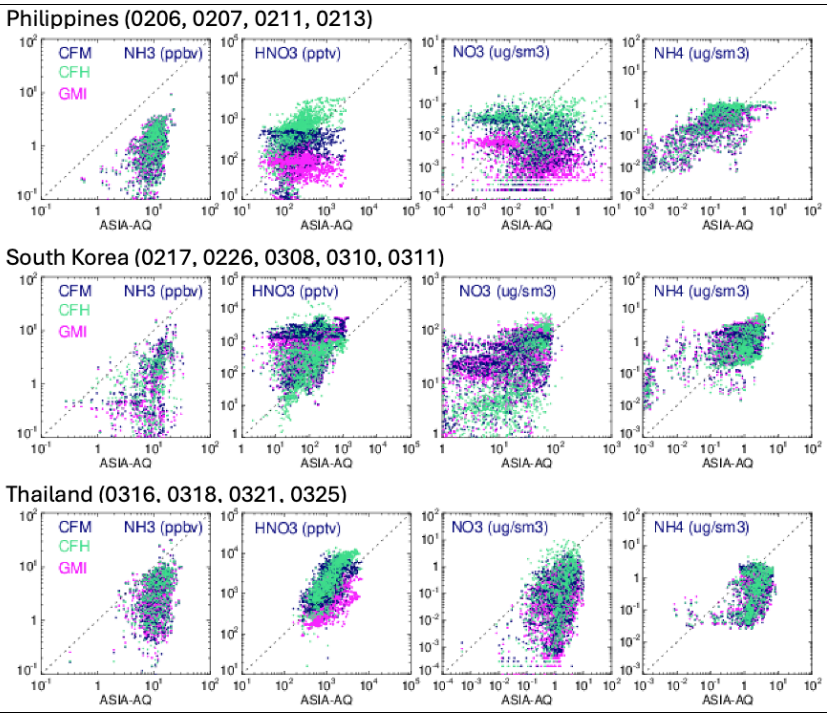


Figure 3. Scatter plots comparing aerosol concentration of nitrate-related species from three GEOS simulations to ASIA-AQ measurements for the flights over the Philippines (top panel), South Korea (middle pane), and Thailand (bottom panel). The corresponding correlation coefficients and ratios of mean tracer concentrations between GEOS simulation results and ASIA-AQ measurements are given in Table 4.

335 **Table 4.** Correlation coefficients (R) and ratios of mean concentrations between model and observation for nitrate-related species during ASIA-AQ (Fig. 3).

		NH_3		HNO_3		NO_3		NH_4	
		R	Ratio [a]	R	Ratio [a]	R	Ratio [a]	R	Ratio [a]
Philippines	CFH	0.50	0.10	0.59	2.24	0.21	0.14	0.47	1.10
	CFM	0.51	0.10	0.00	1.17	0.09	0.07	0.44	1.02
	GMI	0.51	0.11	0.05	0.30	0.08	0.02	0.45	0.93
South Korea	CFH	0.34	0.14	0.39	4.29	0.64	1.34	0.63	1.02
	CFM	0.42	0.16	0.32	7.20	0.56	1.55	0.59	1.10
	GMI	0.39	0.14	0.47	7.72	0.63	1.75	0.63	1.31
Thailand	CFH	0.39	0.32	0.80	2.14	0.27	0.23	0.31	0.32
	CFM	0.38	0.32	0.60	1.74	0.33	0.13	0.20	0.30
	GMI	0.38	0.33	0.48	0.69	0.38	0.07	0.30	0.29

https://doi.org/10.5194/egusphere-2026-5795
Preprint. Discussion started: 11 November 2026
© Author(s) 2026. CC BY 4.0 License.

3.1.2 Example of the impact of temporal variability in oxidant fields on chemical reactions

To illustrate the roles of temporal variability in oxidant fields and the potentially non-linear chemical interactions between oxidants and aerosol precursor gases, we examine the time dimension in greater detail by analyzing the hourly evolution of DMS chemistry during the ASIA-AQ campaign, specifically the first two days of February 2024 over the Philippines (Fig. 4). Specifically, we investigate the responses of DMS to OH and NO_3 radical fields, along with the resulting variations in DMS and MSA concentrations through the following reaction pathways adopted in GOCART-2G:

Reaction	Rate Coefficient (cm^3 molecular $^{-1}$ s^{-1})	Note
$DMS + OH \rightarrow SO_2 + \cdots$	$9.6 \times 10^{-12} \exp\left(-\frac{234}{T}\right)$	$Eq.1$
$DMS + OH \rightarrow 0.75SO_2 + 0.25MSA + \cdots$	$\frac{1.7 \times 10^{-42} \exp\left(\frac{7810}{T}\right)[O_2]}{1 + 5.5 \times 10^{-31} \exp\left(\frac{7460}{T}\right)[O_2]}$	$Eq.2$
$DMS + NO_3 \rightarrow SO_2 + \cdots$	$1.9 \times 10^{-13} \exp\left(\frac{500}{T}\right)$	$Eq.3$

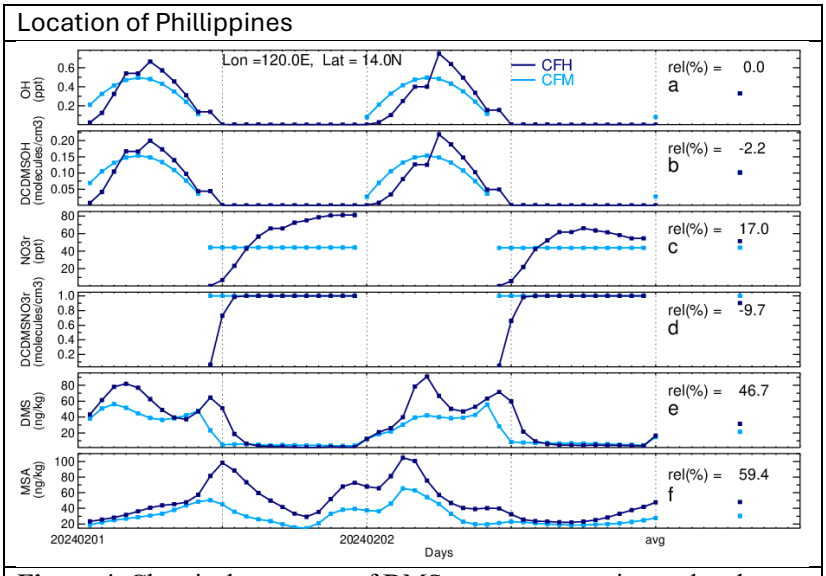


Figure 4. Chemical processes of DMS response to various related fields when using hourly versus monthly oxidant fields at location of Philippines. From top to bottom, the vertical axes represent: OH mixing ratio, OH-driven DMS chemical transformation, NO_3 radical mixing ratio, NO_3 radical-driven DMS transformation, DMS mass mixing ratio, and MSA mass mixing ratio. The location of the Philippines is marked with a open-red-circle in Fig. 6. Here rel (%) = (CFH-CFM)/CFM*100%.

https://doi.org/10.5194/egusphere-2026-5795
Preprint. Discussion started: 11 November 2026
© Author(s) 2026. CC BY 4.0 License.

During the daytime, DMS chemical loss (Fig. 4b) is primarily governed by OH through both hydrogen abstraction (Eq. 1) and OH addition (Eq. 2). This DMS chemical loss closely tracks diurnal OH concentrations (Fig. 4a), peaking at midday, and exhibits a proportional kinetic response. In our hourly-resolved simulation (CFH), lower early-morning OH concentrations (Fig. 4a) slow the initial daytime oxidation of DMS (Fig. 4b) and leave more atmospheric DMS concentration (Fig. 4d) compared to the mean-field simulation (CFM). Overall, DMS chemical conversion in CFH is reduced by approximately 2% relative to CFM over the studied period and location. Because the OH-addition pathway (Eq. 2) is the exclusive route for MSA formation within the GOCART-2G chemical mechanism, atmospheric MSA variation closely follows the pattern of atmospheric DMS.

In contrast, nocturnal DMS oxidation is driven by NO_3 radical and exhibits a distinctly non-linear saturation behavior. While DMS oxidation (Fig. 4d) initially increases with rising evening NO_3 radical levels, the chemical conversion saturates once NO_3 radical concentrations exceed a threshold of approximately ~25 ppt. Further increases in NO_3 radical produce negligible additional DMS oxidation and is limited by the rate of DMS production. Consequently, although the CFH simulation features 17% higher NO_3 radical concentrations than CFM, the resulting DMS conversion through the NO_3 radical pathway is paradoxically 9.7% lower. This saturation effect fundamentally limits the impact of enhanced nighttime NO_3 radical on overall sulfur product formation.

The differing responses to these oxidants dictate the overall atmospheric persistence of DMS. The OH pathway primarily controls daytime atmospheric DMS differences, while NO_3 radical removes nearly all remaining DMS at night. The combination of early-morning OH deficits and nocturnal NO_3 radical saturation in the temporally resolved CFH fields results in a weaker overall chemical conversion compared to simulations utilizing CFM time-averaged oxidant fields, thereby sustaining higher atmospheric DMS concentrations. These findings demonstrate that utilizing monthly (or even daily) mean oxidant fields obscures critical chemical non-linearities, emphasizing the necessity of resolving sub-daily diurnal cycles in oxidant fields to accurately simulate sulfur chemistry and aerosol precursor processing.

Figure 5 illustrates the hourly variations of various gases and aerosols associated with nitrate aerosol formation at the Philippines sampling site over the two-day observation period. In GOCART-2G the coarse mode nitrate is exclusively generated through heterogeneous reactions involving HNO_3 occurring on the surfaces of aerosol particles; in contrast, the formation of fine-mode nitrate (Fig. 5d) is predominantly attributed to thermodynamic equilibrium processes within the NH_3–NH_4^+–NO_3^-–SO_4^{2-} system represented by the Regional Particulate Model Aerosol Reacting System (RPMARES), an inorganic aerosol thermodynamic equilibrium module (Saxena et al., 1986; Bian et al., 2017). Heterogeneous reactions also contribute to the formation of fine mode nitrate. A significant disparity in HNO_3 concentrations (Fig. 5a) can be found between the CFH and CFM approaches, with HNO_3 concentrations at CFH exceeding those at CFM by almost a factor of three. The CFH simulation exhibits large fluctuations in

https://doi.org/10.5194/egusphere-2026-5795
Preprint. Discussion started: 11 November 2026
© Author(s) 2026. CC BY 4.0 License.

HNO_3 concentrations from diurnal chemical dynamics. Meanwhile, unlike NO_3 radical shown above, HNO_3 in CFM is allowed to deplete over a three-hour window in GOCART-2G. However, after three hours the HNO_3 concentration is replenished to its monthly mean value resulting in the small artificial three-hourly oscillations seen in Fig 5a. The elevated HNO_3 concentrations in CFH provided additional acidity for the neutralization reaction of NH_3, resulting in a decrease in NH_3 concentrations (Fig. 5b), and a corresponding increase in concentrations of NH_4 (Fig. 5c) and fine mode and total nitrate aerosols (Fig. 5d-e). Notably, this study reveals yet another instance of nonlinear chemical behavior: the significant increase in HNO_3 concentration under the CFH approach is not proportionally into corresponding change in nitrate (e.g. a 293% increase in HNO_3 yields a 348% increase in fine mode nitrate aerosol). This disproportionate discrepancy between the CFH and CFM simulations also exhibited time-varying characteristics across different nitrate-related species.

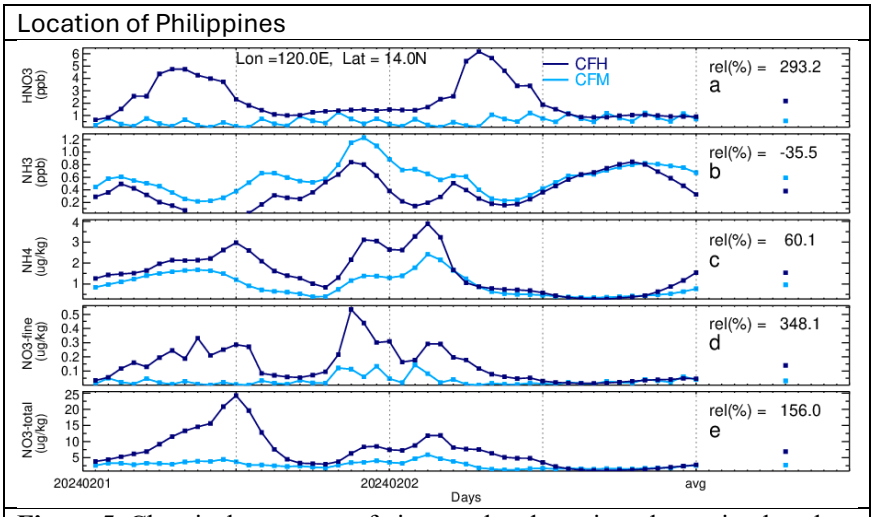


Figure 5. Chemical processes of nitrate-related species when using hourly versus monthly oxidant fields at location of Philippines. Here rel (%) = (CFH-CFM)/CFM*100%.

Similar analysis evaluating sulfate and nitrate formation dynamics over South Korea and Thailand analogous to Figs. 4 & 5 are presented in Figs. S1–4 of the Supplementary Material. Although the magnitudes of the oxidant fields and their consequent chemical impacts differ, the general conclusion remains the same: the high temporal variability of oxidant fields and the nonlinear responses of chemical transformations in CFH lead to elevated atmospheric DMS, MSA, and nitrate aerosol concentrations. This detailed temporal analysis provides clear examples revealing the role of temporal variability within oxidant fields, as well as the potential nonlinear chemical interactions between oxidants and aerosol precursor gases—features that are often obscured when the analysis relies solely on monthly averaged fields. Models that use coarse temporal resolution or averaged oxidant fields on monthly (even daily) scale often miss these

https://doi.org/10.5194/egusphere-2026-5795
Preprint. Discussion started: 11 November 2026
© Author(s) 2026. CC BY 4.0 License.

transitions, leading to biases in both magnitude and composition of aerosol precursors and secondary aerosols.

3.2 2019 Global analysis

3.2.1 Global overview

This section illustrates how the three oxidant fields influence the horizontal and vertical distributions of sulfur- and nitrate-related species on global scales for the year 2019. Figure 6 compares the surface sulfate-related trace gas and aerosol mass concentrations (a1-d1) and the differences between CFH and CFM (a2-d2, pair 1) as well as between GMI and CFM (a3-d3, pair 2), respectively. The CFM (a1-d1) correctly captures the expected spatial distributions of atmospheric sulfur species based on their primary emission sources: DMS and MSA are primarily concentrated over the oceans, particularly in the Southern Ocean, while SO_2 and SO_4 exhibit high concentrations over highly populated and industrialized continental regions. Both DMS and MSA exhibit nearly global enhancements of more than 10% when hourly temporally varying oxidant fields are applied in the CFH simulation (Fig. 6a2 and 4b2). A distinct inverse relationship is observed between SO_2 and SO_4 when switching from CFM to CFH. CFH decreases SO_2 globally by 8% (Fig. 6c2) but increases SO_4 globally by 7% (Fig. 6d2), particularly over major emission regions like East Asia. This pattern strongly suggests that the CFH approach has a more rapid or efficient oxidation conversion from SO_2 to SO_4 compared to CFM. In contrast, despite using the same timing application strategy as CFM, the GMI reduce both DMS and MSA surface total masses by more than 30% (Fig. 6a3 and 4b3), which can be explained by the difference of oxidant fields produced by the MERRA2-GMI and GEOS-CF, respectively, as analyzed in Section 3.2.2 below. These substantial differences are also reflected in the simulated surface SO_2 and SO_4 concentrations, although with smaller magnitudes. The spatial patterns (negative SO_2 and positive SO_4 over Northern Hemisphere land) confirm that, like CFH, the GMI mechanism likely oxidizes SO_2 into SO_4 more aggressively than the CFM approach. Regional impacts are considerably stronger than the corresponding global mean changes in both the pairs, particularly for SO_2 and SO_4 over highly polluted regions.

https://doi.org/10.5194/egusphere-2026-5795
Preprint. Discussion started: 11 November 2026
© Author(s) 2026. CC BY 4.0 License.

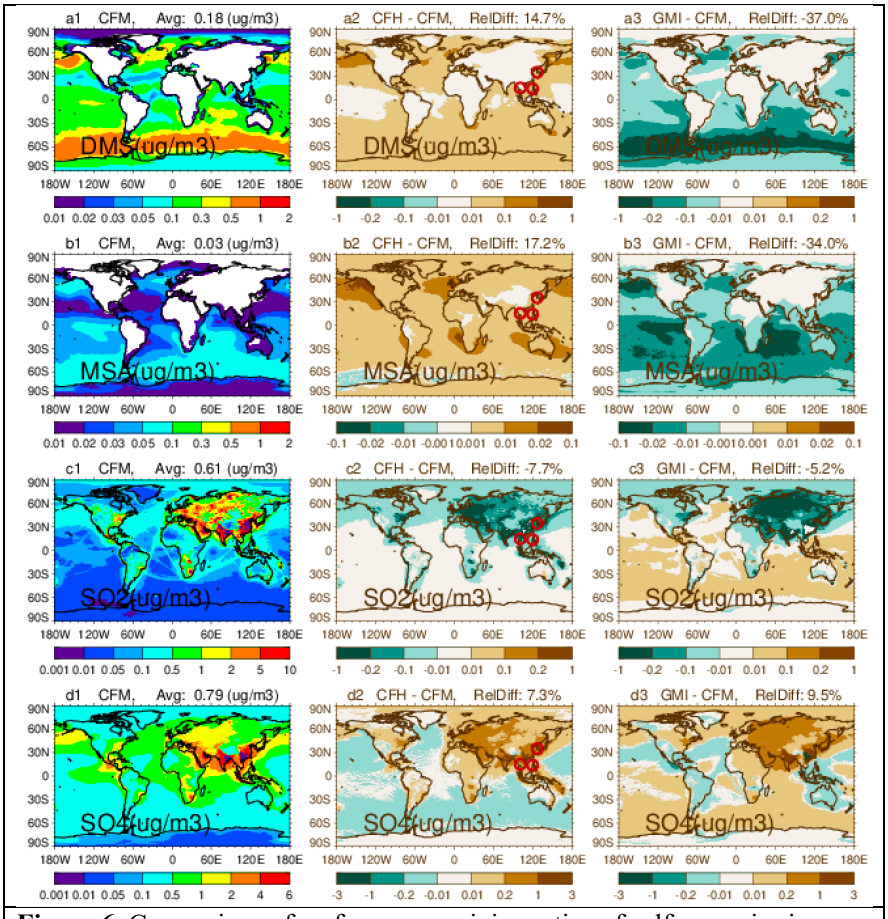


Figure 6. Comparison of surface mass mixing ratios of sulfur species in 2019: (a1-d1) sulfur species simulated by CFM, (a2-d2) absolute differences between CFH and CFM, and (a3-d3) absolute differences between GMI and CFM. The values in the panel titles represent the global mean concentrations for the a1-d1 and the relative differences for a2-d2 (e.g., (CFH-CFM)/CFM)*100%) and a3-d3 (e.g., (GMI-CFM)/CFM*100%). The open-red-circles in a2-d2 indicate the locations where detailed analyses of chemical processes were conducted (as shown in Figs. 4-5, and S1-S4.)

The corresponding zonal mean vertical distributions of sulfur species are shown in Fig. 7. DMS and MSA are primarily confined to the lower troposphere, with maximums in the Southern Ocean (Fig. 7a1-b1). SO_2 has a massive burden in the Northern Hemisphere lower/mid-troposphere due to industrial emissions (Fig. 7c1). Both SO_2 and SO_4 show significant concentrations in the upper troposphere and low stratosphere in the Northern Hemisphere (Fig. 7c1-d1), and DMS and SO_2 show evidence of deep convective lofting in the tropics, reaching the upper troposphere. Figure 7 demonstrates that DMS and MSA are vertically enhanced in CFH by

https://doi.org/10.5194/egusphere-2026-5795
Preprint. Discussion started: 11 November 2026
© Author(s) 2026. CC BY 4.0 License.

more than 20%. The enhancement within the vertical column (Fig. 7a2-b2) exceeded that observed near the surface (Fig. 6a2-b2), indicating that under the CFH mechanism, DMS possesses a longer chemical lifetime, allowing for greater vertical transport via convection before it undergoes oxidation. CFH reduces SO_2 across almost the entire Northern Hemisphere troposphere by 15%. Correspondingly, SO_4 is enhanced by 3% primarily in the lower troposphere. These changes further confirm that CFH drives a much faster oxidation of SO_2 into SO_4 in the lower atmosphere compared to CFM. On the other hand, GMI still significantly decreases DMS and MSA throughout the vertical column, and the magnitude of the reduction is comparable to that observed near the surface. GMI reduces the global SO_2 burden deeply by 17% throughout the SH free troposphere and NH troposphere. Correspondingly, GMI increases SO_4 by 3% mostly concentrated in the lower troposphere near the source regions.

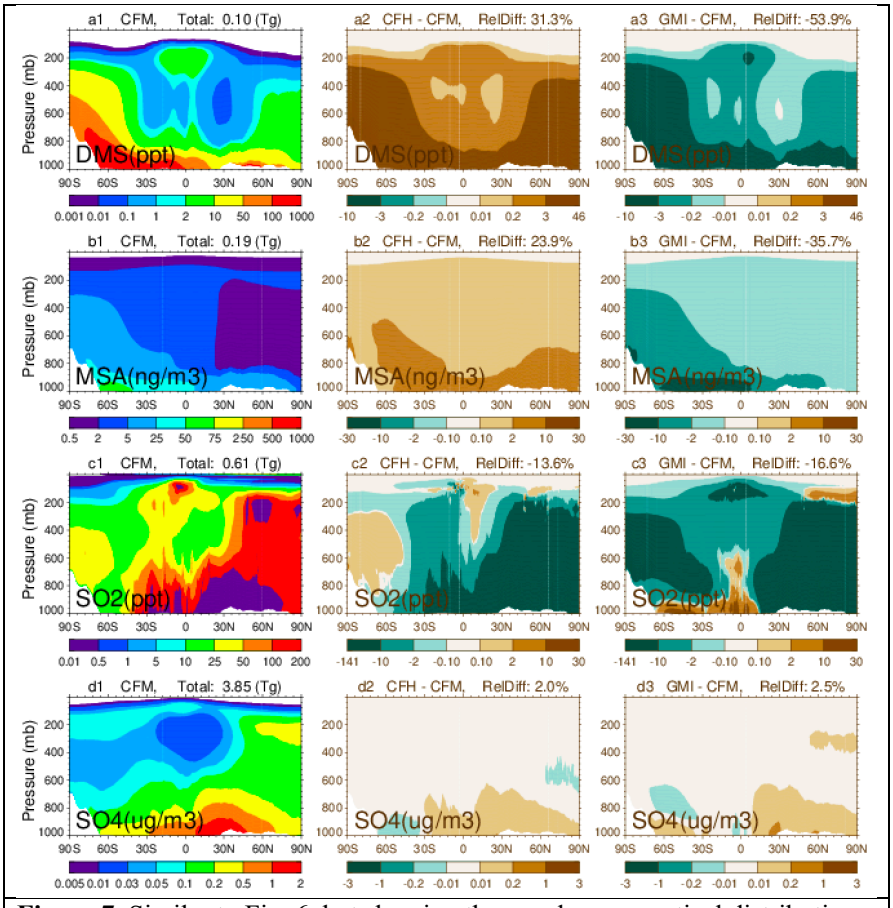


Figure 7. Similar to Fig. 6, but showing the zonal-mean vertical distributions of sulfur species for 2019. The values in the titles represent the global total burdens in a1-d1 and the relative differences in the remaining panels.

https://doi.org/10.5194/egusphere-2026-5795
Preprint. Discussion started: 11 November 2026
© Author(s) 2026. CC BY 4.0 License.

A comparison of surface nitrate-related gas and aerosol mass concentrations among the three experiments is presented in Fig. 8. The CFM simulation represents the spatial distribution of the inorganic nitrogen cycle well, heavily driven by anthropogenic and agricultural activities. Compared to using monthly average oxidant fields, using highly temporally varying oxidant fields shifts the thermodynamic partitioning and oxidation within the nitrogen cycle toward the aerosol phase. Specifically, CFH leads to a 11% increase in global HNO_3, accompanied by a 13% decrease in NH_3 and increases of 30% and 20% in NH_4 and NO_3, respectively. The regional impacts are even more pronounced, particularly over East and Southeast Asia. In contrast, when MERRA2-GMI oxidant fields are applied, surface HNO_3 concentrations become substantially lower (see discussion in Fig. 9), which consequently results in much lower nitrate aerosol production. However, the corresponding changes in NH_3 and NH_4 are relatively minor, likely constrained by the availability of NH_3 and competition with sulfuric aerosols.

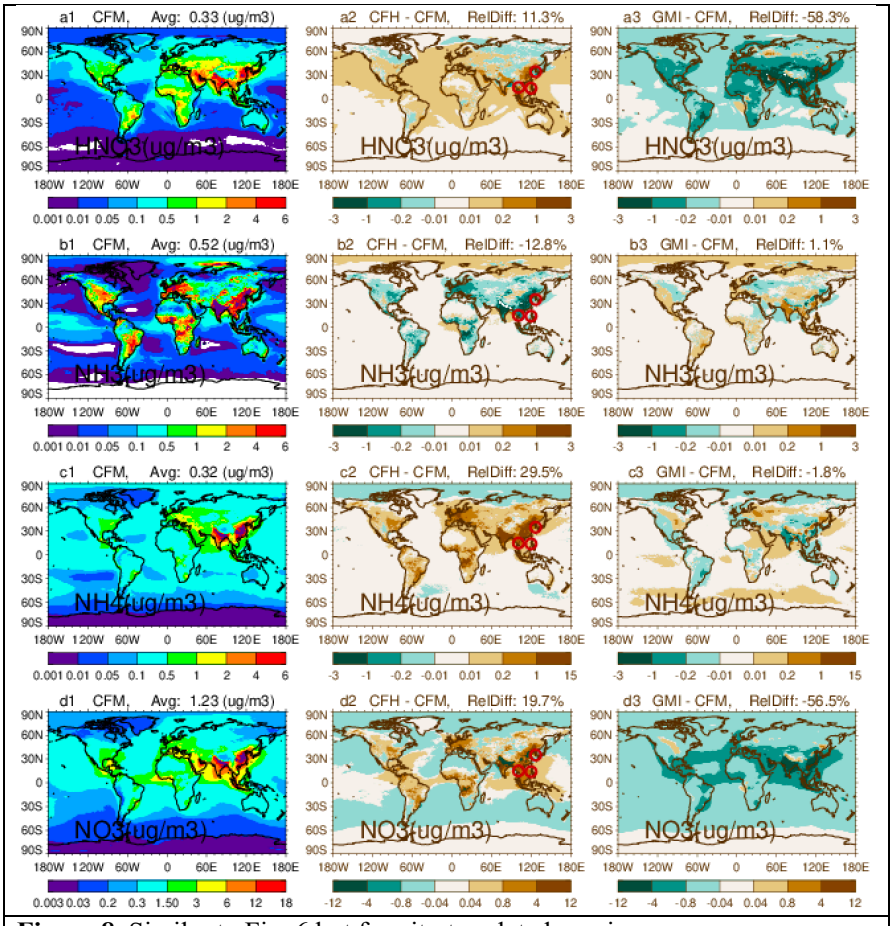


Figure 8. Similar to Fig. 6 but for nitrate-related species.

https://doi.org/10.5194/egusphere-2026-5795
Preprint. Discussion started: 11 November 2026
© Author(s) 2026. CC BY 4.0 License.

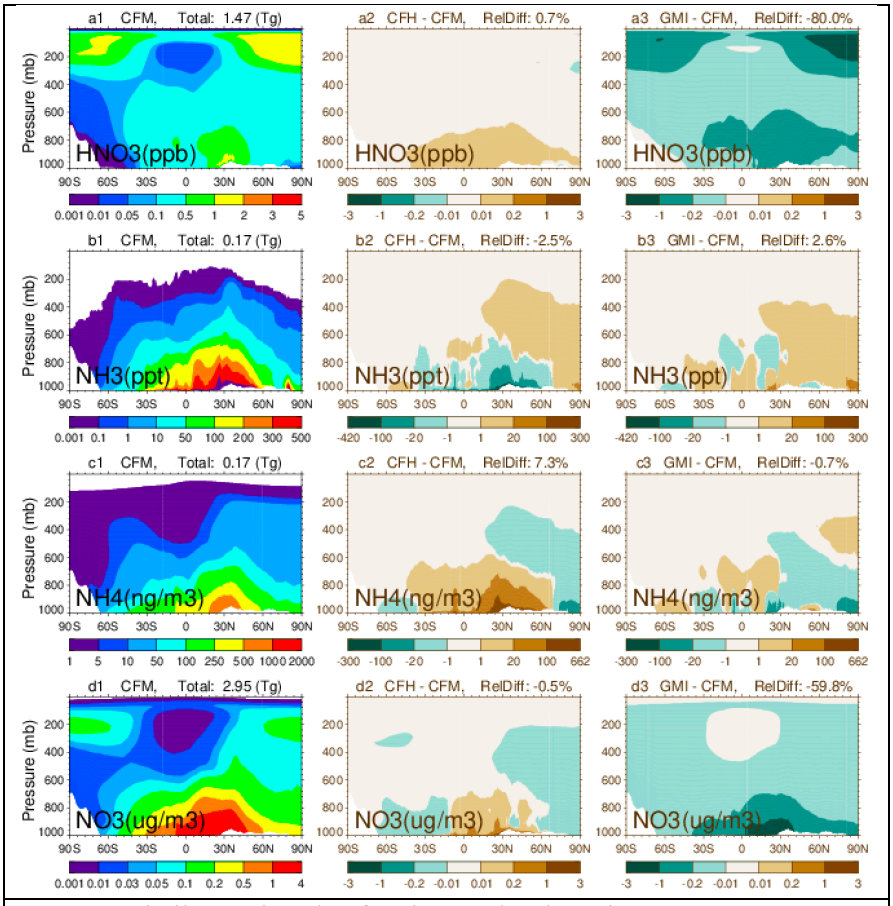


Figure 9. Similar to Fig. 7 but for nitrate-related species.

The zonal mean vertical distributions of nitrate-related species are shown in Fig. 9. Both NH_3 and NH_4 are heavily concentrated in the lower troposphere, primarily in the NH low-to middle latitudes, reflecting their surface-bound agricultural and emission sources and relatively short atmospheric lifetimes. HNO_3 and NO_3 have a much broader vertical and latitudinal spread. When hourly temporally varying oxidant fields are applied, the resulting global single-digit percentage changes in NH_3, NH_4, and NO_3 represent a balance between the large changes occurring near source regions and the comparatively smaller, but opposing, changes elsewhere. Similar as shown in Fig. 8, CFH thermodynamics and kinetics heavily favor the formation of ammonium nitrate aerosols at lower altitudes where precursor concentrations are highest. As also evident in Fig. 8, HNO_3 concentrations in the GMI simulation are substantially lower than those in CFM. As described in Section 2.2, the GMI HNO_3 fields are scaled to compensate for missing nitrate aerosol feedback in the source simulation. Applying a uniform factor also reduces stratospheric HNO_3, where that correction is not targeted. The lower HNO_3 in GMI therefore reflects both its

https://doi.org/10.5194/egusphere-2026-5795
Preprint. Discussion started: 11 November 2026
© Author(s) 2026. CC BY 4.0 License.

source fields and their processing. Lower concentrations than CFM do not alone demonstrate overcorrection against observations; the aircraft comparisons show a region-dependent HNO_3 bias (Table 4).

Figure S5 in the Supplementary Materials illustrates the annual average 550 nm aerosol optical depth and surface PM2.5 (particulate matter with particle diameter < 2.5 μm) mass concentration fields derived from the three experiments. Although the discrepancies among the experimental results for these total aerosol concentration metrics are less than 4% on a global scale, these differences increase significantly at the regional land scale—particularly when utilizing oxidant field data characterized by high temporal variability, which leads to a marked deterioration in simulated air pollution conditions.

3.2.2 Global budget analysis on monthly and annual scales

To obtain a comprehensive picture of the sensitivity of aerosol formation to different representations of oxidant fields, we conduct a monthly budget analysis on a global scale for the year 2019. Figure 10 shows the impacts of applying the three oxidant fields on monthly global burdens, surface concentrations, and chemical production of sulfur species (e.g., DMS, MSA, SO_2, and SO_4), as well as the associated oxidants (e.g., OH, NO_3 radicals, and H_2O_2). Oxidants generated from the same chemical mechanism but using different temporal averaging strategies (CFH vs. CFM; relative difference defined as (CFH-CFM)/CFM*100%) exhibit considerably small differences. However, the resulting differences in simulated sulfur species are not proportionally reduced compared with those in the oxidant fields, indicating that sulfur chemistry responds nonlinearly to temporal variations in oxidants. This interpretation is further supported by the chemical budget analysis, which shows that differences in CFH versus CFM are often comparable to, and in some cases even larger than, those in GMI versus CFM. These results suggest that temporal variability and nonlinear chemical feedback play important roles in controlling sulfur species formation beyond what would be expected from differences in oxidant abundance alone. The overall global 2019 budgets, mean surface concentrations, and contributions from chemical and physical processes from the three oxidant experiments for sulfur species are summarized in Table S1. The use of oxidant field data with higher temporal resolution results in an increase of more than 20% in the global burdens of DMS and MSA, with this enhancement persisting throughout the year (Fig. 10L0–1 and Table S1). This chemical response of DMS is consistent with changes in the concentrations of OH and NO_3 radicals—the primary oxidants involved in DMS oxidation—and further corroborates the nonlinear chemical response of DMS to transient oxidant fields, as illustrated in Fig. 6. The behavior of SO_2, however, is more complex. In the CFH scenario, the increased DMS burden indicates a weakening of the DMS oxidation process, which consequently reduces the production of gas-phase SO_2 (Fig. 10C1). At the same time, the oxidative conversion of SO_2 to sulfate is enhanced in the CFH scenario, as evidenced by the positive relative difference of CFH versus CFM values corresponding to SO_4 (Fig. 10C3). The combined effects of reduced SO_2 production and

https://doi.org/10.5194/egusphere-2026-5795
Preprint. Discussion started: 11 November 2026
© Author(s) 2026. CC BY 4.0 License.

enhanced SO_2 chemical conversion therefore lead to a further decrease in the SO_2 burden under the CFH scenario.

In contrary, oxidants produced from two different sources of the simulated oxidant fields (MERRA2-GMI vs. GEOS-CF) show substantial differences in both global surface concentrations and column burdens (Fig. 10L4-6 and Fig. 10S4-6), leading to pronounced discrepancies in the simulated sulfur species. The differences for DMS and MSA are particularly large, with the relative difference (defined as (GMI-CFM)/CFM*100%) typically exceeds 30% on both surface levels or total column burdens.

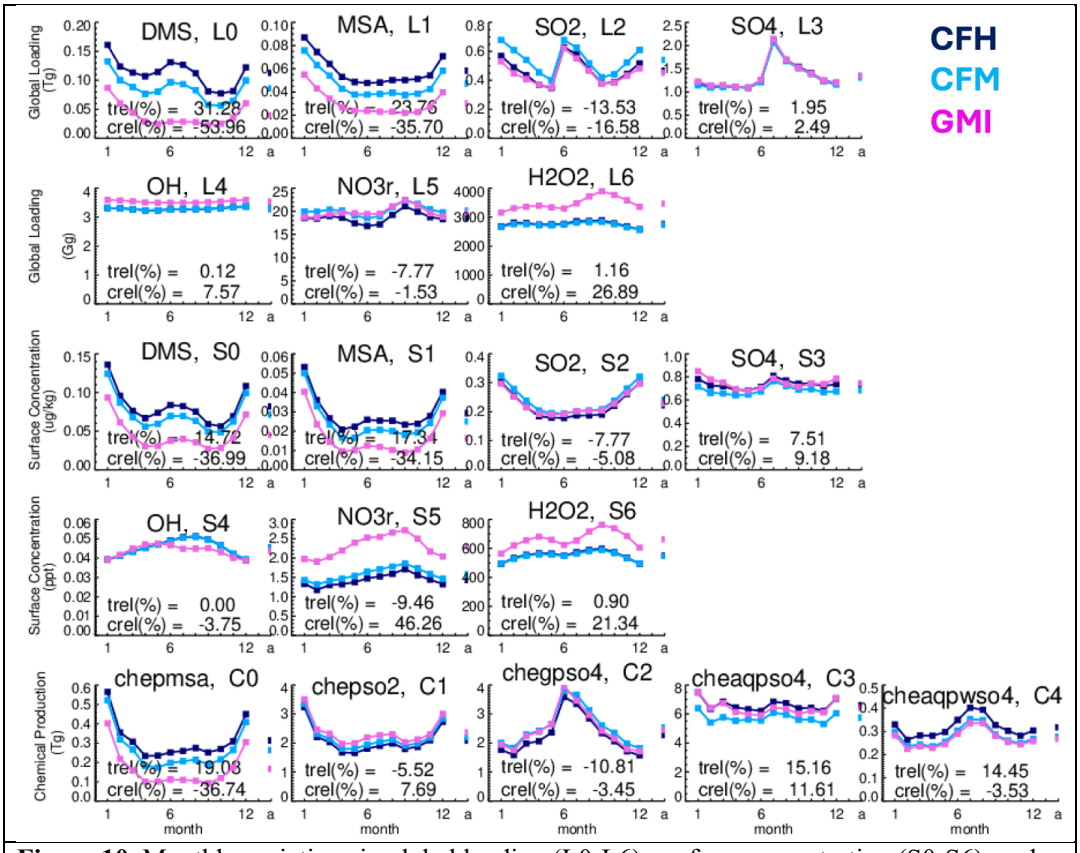


Figure 10. Monthly variations in global loading (L0-L6), surface concentration (S0-S6), and chemical transformation (C0-C4) of sulfur species and their precursors from simulations of the application of three oxidants. Specifically, C0–C2 represent the gas-phase formation of MSA (chepmsa), SO_2 (chepso2), and SO_4 (chegpso4), respectively, while C3-4 represent the aqueous-phase formation of SO_4 in clouds (cheaqpso4) and during wet deposition (cheaqwso4), respectively. Here trel = (CFH – CFM) / CFM *100% and crel = (GMI – CFM) / CFM *100%.

https://doi.org/10.5194/egusphere-2026-5795
Preprint. Discussion started: 11 November 2026
© Author(s) 2026. CC BY 4.0 License.

Figure 11 shows the impacts of the three oxidant fields on nitrate species (e.g., NH_3, NH_4, NO_3), as well as the associated oxidant, HNO_3, with the GMI experiment exhibiting substantially lower HNO_3 levels. As discussed in Fig. 9, applying a uniform global scaling factor excessively reduces stratospheric HNO_3 used by GMI. As a result, the relative difference of GMI versus CFM for whole atmosphere HNO_3 becomes extraordinarily large. Excluding stratospheric HNO_3, the relative difference decreases from −80.1% to −69.8%, as expected. The negative tropospheric relative difference indicates that the calibrated GMI HNO_3 remains lower than that in CFM, leading to lower simulated aerosol nitrate concentrations, primarily because of reduced heterogeneous reactions of HNO_3 with dust and sea salt, as reflected by the negative relative difference of GMI versus CFM in Fig. 11C3. In contrast, aerosol nitrate chemical production calculated through the thermodynamic equilibrium model for the NH_3–NH_4^+–NO_3^-–SO_4^{2-} system is significantly higher in the GMI experiment and exhibits a notably different seasonal cycle than the CFM experiment (Fig. 11C2), reflecting enhanced partitioning toward aerosol nitrate formation. Because the lower HNO_3 concentrations in GMI require less NH_3 for neutralization, gaseous NH_3 remains higher while particulate NH_4^+ is correspondingly lower in GMI compared with CFM. On the other hand, the CFH–CFM differences in nitrate-related species arise primarily from thermodynamic equilibrium processes (Fig. 11 C0-3). Table S2 summarizes the annual global nitrate budgets, mean surface concentrations, and chemical and physical process contributions for all three experiments.

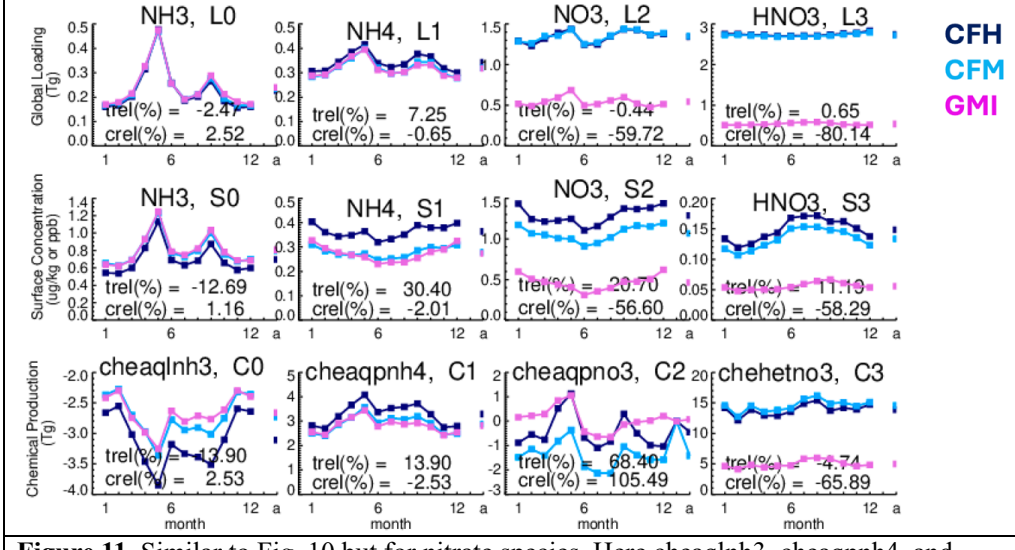


Figure 11. Similar to Fig. 10 but for nitrate species. Here cheaqlnh3, cheaqpnh4, and cheaqpno3 represent the chemical loss of NH_3 and the chemical production of NH_4 and NO_3, respectively, occurring via thermodynamic equilibrium, while chehetno3 represents the production of NO_3 through heterogeneous reactions of HNO_3 on the surfaces of dust and sea-salt aerosols. Unit of surface concentration is μg/kg for aerosols and ppb for gases.

https://doi.org/10.5194/egusphere-2026-5795
Preprint. Discussion started: 11 November 2026
© Author(s) 2026. CC BY 4.0 License.

4. Conclusion

Accurately simulating secondary inorganic aerosols, such as sulfate and nitrate, requires a detailed representation of complex atmospheric oxidant chemistry. However, global models such as the GEOS GOCART-2G aerosol module—widely used by the community, including in the MERRA-2 reanalysis—typically employ a decoupled approach in which aerosol chemistry is driven by monthly mean oxidant fields. While computationally efficient, this design overlooks the high-frequency temporal variability and nonlinear interactions inherent in aerosol–oxidant chemistry. In this study, we systematically evaluated the sensitivity of GOCART-2G aerosol simulations to different oxidant field representations by comparing three configurations: hourly GEOS-Chem oxidants (CFH), monthly mean GEOS-Chem oxidants (CFM), and the default monthly mean GMI-Chem oxidants (GMI). The model was evaluated against regional airborne measurements from the 2024 ASIA-AQ campaign and through a global chemical budget analysis for 2019.

Our regional analysis during the ASIA-AQ campaign across the Philippines, South Korea, and Thailand demonstrated that utilizing hourly, time-varying oxidant fields improves the correlation of simulated oxidant, sulfate, and nitrate fields with observations compared to that using monthly averages. Despite these improvements, the model-to-observation comparisons revealed persistent limitations in the current GOCART-2G modeling framework. Specifically, precursor emissions require critical reassessment: modeled DMS was severely overestimated over open oceans, while NH_3 was systematically underestimated across all regions regardless of the oxidant field used.

On a global and annual scale, comparison of the CFH and CFM simulations reveals the profound impact of temporal averaging on nonlinear chemical transformations. Monthly averaged chemical fields not only suppresses short-term variability but also alters the nonlinear coupling among reactants and products. Because reaction rates and multiphase processes depend nonlinearly on instantaneous chemical conditions, chemistry driven by monthly mean fields is not necessarily equivalent to the temporal average of chemistry driven by dynamically evolving fields. Our study indicates that because altering the temporal covariance between DMS and its oxidants, the time-varying oxidants shows a weakened chemical transformation of DMS, resulting in a roughly 20% increase in the global DMS and MSA burdens compared to monthly mean oxidants. Corresponding global changes in SO_2 (decrease) and SO_4 (increase) remain minor, as regional decreases and increases largely offset one another. For nitrate-related species, the introduction of temporal variability in CFH exerts a more pronounced influence in the lower troposphere; specifically, its impact on surface nitrate-related species typically ranges between 10% and 20%, whereas the corresponding influence on global burdens diminishes to single-digit percentages.

Furthermore, comparing oxidant fields from the GMI-Chem and GEOS-Chem mechanisms reveals significant structural differences. Because the GMI and CFM approaches use the same strategy to update oxidant fields, discrepancies in their simulated aerosol results stem directly

https://doi.org/10.5194/egusphere-2026-5795
Preprint. Discussion started: 11 November 2026
© Author(s) 2026. CC BY 4.0 License.

from differences in oxidant magnitudes and spatial distributions. Specifically, compared to GEOS-Chem, the GMI-Chem mechanism yields OH concentrations that are approximately 8% higher, NO_3 levels 2% lower, and H_2O_2 levels 27% higher. Consequently, GMI simulates global DMS and MSA concentrations that are over 30% lower. Additionally, because it lacks interactive aerosol feedback, the GMI-Chem mechanism inherently overestimates tropospheric HNO_3. The uniform global scaling factor currently used causes an over-correction in the lower troposphere, resulting in HNO_3 levels that are drastically lower than those produced by the CFM approach.

Ultimately, these findings reveal a significant opportunity to advance the next generation of offline aerosol modeling. While utilizing decoupled, monthly mean oxidant fields has historically provided the computational efficiency necessary for near-real-time forecasting and long-term reanalysis (such as MERRA-2), the experimental results indicate that moving toward dynamic oxidant fields is the logical next step to capture the vital, transient oxidant–aerosol interactions that drive secondary aerosol formation. Based on these findings, we propose that—at least for near-real-time forecasting—GEOS-FP should shift to using high-frequency oxidant fields from GEOS-CF forecasts to drive its GOCART-2G chemistry module. This strategy leverages existing architecture to incorporate time-varying chemical environments and coupled feedback mechanisms, while avoiding the heavy computational burden associated with fully online, interactive chemistry systems.

Code availability

The GEOS Earth System Model source code and the instructions for model build are available at https://github.com/GEOS-ESM/GEOSgcm/ (Last accessed: September 21, 2026).

Data availability. The ASIA-AQ data was obtained from https://www-air.larc.nasa.gov/missions/asia-aq/index.html (last accessed: September 21, 2026).

Author contributions

HB led the writing of the manuscript by preparing the initial draft, with further writing contributions from PC and AC. HB, PC, and AC conceived the study, designed the methodology, performed model simulations, and analyzed and interpreted the results. AD participated in the design of the methodology; PW, RB, and JC participated in revising the manuscript. RG and PW assisted with model simulations; EA, KB, RB, JC, YC, JJ, RM, MZ, and JHC provided ASIA-AQ airborne observational data. All authors reviewed and approved the final manuscript.

Competing interests

None.

Acknowledgements

We thank Peter R. Colarco for assistance with the GEOS model budget analysis and Paul Wennburg for providing the gas tracer measurements. Computing resources supporting this work were provided by the NASA High-End Computing (HEC) Program through the NASA Center for Climate Simulation (NCCS).

https://doi.org/10.5194/egusphere-2026-5795
Preprint. Discussion started: 11 November 2026
© Author(s) 2026. CC BY 4.0 License.

Financial support
This research was supported by NASA through the ASIA-AQ project (22-ASIAAQ22-0003) and the Atmospheric Composition Modeling and Analysis Program (grant no. 80NSSC23K1000). The OPALS ammonia measurements and analyses were supported by NASA (grant no. 80NSSC23K0815).

References

Alexander, B., Park, R. J., Jacob, D. J., Li, Q. B., Yantosca, R. M., Savarino, J., Lee, C. C. W., and Thiemens, M. H.: Sulfate formation in sea-salt aerosols: Constraints from oxygen isotopes, J. Geophys. Res., 110, D10307, https://doi.org/10.1029/2004JD005659, 2005.

Aw, J. and Kleeman, M. J.: Evaluating the first-order effect of intraannual temperature variability on urban air pollution, J. Geophys. Res. Atmos., 108, 4365, https://doi.org/10.1029/2002JD002688, 2003.

Bellouin, N., Quaas, J., Gryspeerdt, E., Kinne, S., Stier, P., Watson-Parris, D., et al.: Bounding global aerosol radiative forcing of climate change, Rev. Geophys., 58, e2019RG000660, https://doi.org/10.1029/2019RG000660, 2020.

Bian, H., Chin, M., Colarco, P. R., Apel, E. C., Blake, D. R., Froyd, K., Hornbrook, R. S., Jimenez, J., Jost, P. C., Lawler, M., Liu, M., Lund, M. T., Matsui, H., Nault, B. A., Penner, J. E., Rollins, A. W., Schill, G., Skeie, R. B., Wang, H., Xu, L., Zhang, K., and Zhu, J.: Observationally constrained analysis of sulfur cycle in the marine atmosphere with NASA ATom measurements and AeroCom model simulations, Atmos. Chem. Phys., 24, 1717–1741, https://doi.org/10.5194/acp-24-1717-2024, 2024.

Bian, H., Chin, M., Hauglustaine, D. A., Schulz, M., Myhre, G., Bauer, S. E., Lund, M. T., Karydis, V. A., Kucsera, T. L., Pan, X., Pozzer, A., Skeie, R. B., Steenrod, S. D., Sudo, K., Tsigaridis, K., Tsimpidi, A. P., and Tørseth, K.: Investigation of global particulate nitrate from the AeroCom phase III experiment, Atmos. Chem. Phys., 17, 12911–12940, https://doi.org/10.5194/acp-17-12911-2017, 2017.

Bian, H., Froyd, K., Murphy, D. M., Dibb, J., Darmenov, A., Chin, M., Colarco, P. R., da Silva, A., Kucsera, T. L., Schill, G., Yu, H., Bui, T. P., Dollner, M., Weinzierl, B., and Smirnov, A.: Observationally constrained analysis of sea salt aerosol in the marine atmosphere, Atmos. Chem. Phys., 19, 10773–10785, https://doi.org/10.5194/acp-19-10773-2019, 2019.

Brown, S. S. and Stutz, J.: Nighttime radical observations and chemistry, Chem. Soc. Rev., 41, 6405–6447, https://doi.org/10.1039/C2CS35181A, 2012.

Carlton, A. G., de Gouw, J., Jimenez, J. L., Ambrose, J. L., Brown, S. S., Baker, K. R., Brock, C. A., Cohen, R. C., Craig, S., Darisse, N. P., and Dickinson, W. H.: Synthesis of the Southeast Atmosphere Studies: Investigating fundamental atmospheric chemistry questions, Bull. Am. Meteorol. Soc., 99, 547–567, https://doi.org/10.1175/BAMS-D-16-0048.1, 2018.

Carn, S. A., Fioletov, V. E., McLinden, C. A., Li, C., and Krotkov, N. A.: A decade of global volcanic SO2 emissions measured from space, Sci. Rep., 7, 44095, https://doi.org/10.1038/srep44095, 2017.

Chin, M., Diehl, T., Dubovik, O., Eck, T. F., Holben, B. N., Sinyuk, A., and Streets, D. G.: Light absorption by pollution, dust, and biomass burning aerosols: a global model study and evaluation with AERONET measurements, Ann. Geophys., 27, 3439–3464, https://doi.org/10.5194/angeo-27-3439-2009, 2009.

https://doi.org/10.5194/egusphere-2026-5795
Preprint. Discussion started: 11 November 2026
© Author(s) 2026. CC BY 4.0 License.



Chin, M., Diehl, T., Tan, Q., Prospero, J. M., Kahn, R. A., Remer, L. A., Yu, H., Sayer, A. M., Bian, H., Geogdzhayev, I. V., Holben, B. N., Howell, S. G., Huebert, B. J., Hsu, N. C., Kim, D., Kucsera, T. L., Levy, R. C., Mishchenko, M. I., Pan, X., Quinn, P. K., Schuster, G. L., Streets, D. G., Strode, S. A., Torres, O., and Zhao, X.-P.: Multi-decadal aerosol variations from 1980 to 2009: a perspective from observations and a global model, Atmos. Chem. Phys., 14, 3657–3690, https://doi.org/10.5194/acp-14-3657-2014, 2014.

Chin, M., Ginoux, P., Kinne, S., Torres, O., Holben, B. N., Duncan, B. N., Martin, R. V., Logan, J. A., Higurashi, A., and Nakajima, T.: Tropospheric aerosol optical thickness from the GOCART model and comparisons with satellite and Sun photometer measurements, J. Atmos. Sci., 59, 461–483, https://doi.org/10.1175/1520-0469(2002)059<0461:TAOTFT>2.0.CO;2, 2002.

Chin, M., Jacob, D. J., Gardner, G. M., Foreman-Fowler, M. S., Spiro, P. A., and Savoie, D. L.: A global three-dimensional model of tropospheric sulfate, J. Geophys. Res., 101, 18667, https://doi.org/10.1029/96jd01221, 1996.

Colarco, P., da Silva, A., Chin, M., and Diehl, T.: Online simulations of global aerosol distributions in the NASA GEOS-4 model and comparisons to satellite and ground-based aerosol optical depth, J. Geophys. Res., 115, D14207, https://doi.org/10.1029/2009JD012820, 2010.

Collow, A. B., Colarco, P. R., da Silva, A. M., Buchard, V., Bian, H., Chin, M., Das, S., Govindaraju, R., Kim, D., and Aquila, V.: Benchmarking GOCART-2G in the Goddard Earth Observing System (GEOS), Geosci. Model Dev., 17, 1443–1468, https://doi.org/10.5194/gmd-17-1443-2024, 2024.

Crawford, J. H., et al.: Airborne and Satellite Investigation of Asian Air Quality (ASIA-AQ) White Paper/Science Plan, NASA, https://espo.nasa.gov/asia-aq, 2022.

Darmenov, A. S. and da Silva, A. M.: The Quick Fire Emissions Dataset (QFED): Documentation of versions 2.1, 2.2 and 2.4, NASA Technical Report Series on Global Modeling and Data Assimilation, Vol. 38, NASA/TM-2015-104606, Goddard Space Flight Center, Greenbelt, Maryland, USA, https://ntrs.nasa.gov/citations/20180005253, 2015.

Ervens, B.: Modeling the processing of aerosol and trace gases in clouds and aerosols, Chem. Rev., 115, 4157–4198, https://doi.org/10.1021/cr5005887, 2015.

Forster, P., Storelvmo, T., Armour, K., Collins, W., Dufresne, J.-L., Frame, D., Lunt, D. J., Mauritsen, T., Palmer, M. D., Watanabe, M., Wild, M., and Zhang, H.: The Earth's energy budget, climate feedbacks, and climate sensitivity, in: Climate Change 2021: The Physical Science Basis. Contribution of Working Group I to the Sixth Assessment Report of the Intergovernmental Panel on Climate Change, edited by: Masson-Delmotte, V., et al., Cambridge University Press, Cambridge, United Kingdom and New York, NY, USA, 923–1054, https://doi.org/10.1017/9781009157896.009, 2021.

Fuzzi, S., et al.: Particulate matter, air quality and climate: lessons learned and future needs, Atmos. Chem. Phys., 15, 8217–8299, https://doi.org/10.5194/acp-15-8217-2015, 2015.

https://doi.org/10.5194/egusphere-2026-5795
Preprint. Discussion started: 11 November 2026
© Author(s) 2026. CC BY 4.0 License.

Gelaro, R., McCarty, W., Suárez, M. J., Todling, R., Molod, A., Takacs, L., Randles, C. A., Darmenov, A., Bosilovich, M. G., Reichle, R., Wargan, K., Coy, L., Cullather, R., Draper, C., Akella, S., Buchard, V., Conaty, A., da Silva, A. M., Gu, W., Kim, G.-K., Koster, R., Lucchesi, R., Merkova, D., Nielsen, J. E., Partyka, G., Pawson, S., Putman, W., Rienecker, M., Schubert, S. D., Sienkiewicz, M., and Zhao, B.: The Modern-Era Retrospective Analysis for Research and Applications, Version 2 (MERRA-2), J. Clim., 30, 5419–5454, https://doi.org/10.1175/JCLI-D-16-0758.1, 2017.

Hoesly, R. M., Smith, S. J., Feng, L., Klimont, Z., Janssens-Maenhout, G., Pitkanen, T., Seibert, J. J., Vu, L., Andres, R. J., Bolt, R. M., Bond, T. C., Dawidowski, L., Kholod, N., Kurokawa, J.-I., Li, M., Liu, L., Lu, Z., Moura, M. C. P., O'Rourke, P. R., and Zhang, Q.: Historical (1750–2014) anthropogenic emissions of reactive gases and aerosols from the Community Emissions Data System (CEDS), Geosci. Model Dev., 11, 369–408, https://doi.org/10.5194/gmd-11-369-2018, 2018.

Holmes, C. D., Bertram, T. H., Confer, K. L., Graham, K. A., Ronan, A. C., Wirks, C. K., and Shah, V.: The role of clouds in the tropospheric NOx cycle: A new modeling approach for cloud chemistry and its global implications, Geophys. Res. Lett., 46, 4980–4990, https://doi.org/10.1029/2019GL081990, 2019.

Hu, L., Keller, C. A., Long, M. S., Sherwen, T., Auer, B., Da Silva, A., Nielsen, J. E., Pawson, S., Thompson, M. A., Trayanov, A. L., Travis, K. R., Grange, S. K., Evans, M. J., and Jacob, D. J.: Global simulation of tropospheric chemistry at 12.5 km resolution: performance and evaluation of the GEOS-Chem chemical module (v10-1) within the NASA GEOS Earth system model (GEOS-5 ESM), Geosci. Model Dev., 11, 4603–4620, https://doi.org/10.5194/gmd-11-4603-2018, 2018.

Jacob, D. J.: Heterogeneous chemistry and tropospheric ozone, Atmos. Environ., 34, 2131–2159, https://doi.org/10.1016/S1352-2310(99)00462-8, 2000.

Jacobson, M. Z.: Global direct radiative forcing due to multicomponent anthropogenic and natural aerosols, J. Geophys. Res., 106, 1551–1568, https://doi.org/10.1029/2000JD900514, 2001.

Jeong, J. I., Park, R. J., Kim, C.-H., Song, C.-K., Song, C. H., Kim, S., Woo, J.-H., Emmons, L. K., Saide, P. E., Carmichael, G. R., Pfister, G., Castellanos, P., Miyazaki, K., Lin, H., Malings, C., Kim, H., Lee, S., Lee, G. T., Lee, H.-J., Baek, S.-H., Cha, Y., Yu, J., Han, K. M., Jeong, S., Kim, E., Kim, J., Gaubert, B., Mohanty, M. R., Kim, H., Kumar, R., Bian, H., Collow, A., Choi, J., Sekiya, T., Chang, L.-S., Travis, K. R., and Crawford, J. H.: Multi-model evaluation of winter air quality simulations during the ASIA-AQ campaign in South Korea, Atmos. Environ., ATMENV-D-26-01510, submitted, 2026.

Keller, C. A., Knowland, K. E., Duncan, B. N., Liu, J., Anderson, D. C., Das, S., Lucchesi, R. A., Lundgren, E. W., Nicely, J. M., Nielsen, J. E., Ott, L. E., Saunders, E., Strode, S. A., Wales, P. A., Jacob, D. J., and Pawson, S.: Description of the NASA GEOS composition forecast modeling system GEOS-CF v1.0, J. Adv. Model. Earth Sy., 13, e2020MS002413, https://doi.org/10.1029/2020MS002413, 2021.

Lana, A., Bell, T. G., Simó, R., Vallina, S. M., Dixon, J., Becker, S., et al.: An updated climatology of surface dimethlysulfide concentrations and emission fluxes in the global ocean, Global Biogeochem. Cy., 25, GB1004, https://doi.org/10.1029/2010GB003850, 2011.

https://doi.org/10.5194/egusphere-2026-5795
Preprint. Discussion started: 11 November 2026
© Author(s) 2026. CC BY 4.0 License.

Liss, P. S. and Merlivat, L.: Air–sea gas exchange rates: Introduction and synthesis, in: The Role of Air–Sea Exchange in Geochemical Cycling, D. Reidel Publishing Company, 113–127, https://doi.org/10.1007/978-94-009-4738-2_5, 1986.

Long, M. S., Yantosca, R., Nielsen, J. E., Keller, C. A., da Silva, A., Sulprizio, M. P., Pawson, S., and Jacob, D. J.: Development of a grid-independent GEOS-Chem chemical transport model (v9-02) as an atmospheric chemistry module for Earth System Models, Geosci. Model Dev., 8, 595–602, https://doi.org/10.5194/gmd-8-595-2015, 2015.

Mann, G. W., Carslaw, K. S., Spracklen, D. V., Ridley, D. A., Manktelow, P. T., Chipperfield, M. P., Pickering, S. J., and Johnson, C. E.: Description and evaluation of GLOMAP-mode: a modal global aerosol microphysics model for the UKCA composition-climate model, Geosci. Model Dev., 3, 519–551, https://doi.org/10.5194/gmd-3-519-2010, 2010.

McDuffie, E. E., Fibiger, D. L., Dubé, W. P., Lopez Hilfiker, F., Lee, B. H., Jaeglé, L., et al.: ClNO2 yields from aircraft measurements during the 2015 WINTER campaign and critical evaluation of the current parameterization, J. Geophys. Res.-Atmos., 123, 12994–13015, https://doi.org/10.1029/2018JD029358, 2018.

Nielsen, J. E., Pawson, S., Molod, A., Auer, B., da Silva, A. M., Douglass, A. R., Duncan, B., Liang, Q., Manyin, M., Oman, L. D., Ott, L., Steenrod, S., Strahan, S., and Wargan, K.: Chemical mechanisms and their applications in the Goddard Earth Observing System (GEOS) earth system model, J. Adv. Model. Earth Sy., 9, 3019–3044, https://doi.org/10.1002/2017MS001011, 2017.

Norman, O. G., Heald, C. L., Bililign, S., Campuzano-Jost, P., Coe, H., Fiddler, M. N., Green, J. R., Jimenez, J. L., Kaiser, K., Liao, J., Middlebrook, A. M., Nault, B. A., Nowak, J. B., Schneider, J., and Welti, A.: Exploring the processes controlling secondary inorganic aerosol: evaluating the global GEOS-Chem simulation using a suite of aircraft campaigns, Atmos. Chem. Phys., 25, 771–795, https://doi.org/10.5194/acp-25-771-2025, 2025.

O'Rourke, P. R., Smith, S. J., Mott, A., Ahsan, H., McDuffie, E. E., Crippa, M., Klimont, Z., McDonald, B., Wang, S., Nicholson, M. B., Feng, L., and Hoesly, R. M.: CEDS v_2021_04_21 Release Emission Data, version v_2021_02_05, Zenodo [data set], https://doi.org/10.5281/zenodo.4741285, 2021.

Orbe, C., Oman, L. D., Strahan, S. E., Waugh, D. W., Pawson, S., Takacs, L. L., and Molod, A. M.: Large-scale atmospheric transport in GEOS replay simulations, J. Adv. Model. Earth Sy., 9, 2545–2560, https://doi.org/10.1002/2017MS001053, 2017.

Paulot, F., Fan, S., and Horowitz, L. W.: Contrasting seasonal responses of sulfate aerosols to declining SO2 emissions in the Eastern US: Implications for the efficacy of SO2 emission controls, Geophys. Res. Lett., 44, 455–464, https://doi.org/10.1002/2016GL070695, 2017.

Pye, H. O. T., Nenes, A., Alexander, B., Ault, A. P., Barth, M. C., Clegg, S. L., Collett Jr., J. L., Fahey, K. M., Hennigan, C. J., Herrmann, H., Kanakidou, M., Kelly, J. T., Iinuma, Y., McNeill, V. F., Riemer, N., Schaefer, T., Shi, G., Tilgner, A., Walker, J. T., Wang, T., Weber, R., Xing, J., Zaveri, R. A., and Zuend, A.: The acidity of atmospheric particles and clouds, Atmos. Chem. Phys., 20, 4809–4888, https://doi.org/10.5194/acp-20-4809-2020, 2020.

Randles, C. A., da Silva, A. M., Buchard, V., Colarco, P. R., Darmenov, A., Govindaraju, R., Smirnov, A., Holben, B., Ferrare, R., Hair, J., Shinozuka, Y., and Flynn, C. J.: The MERRA-2

https://doi.org/10.5194/egusphere-2026-5795
Preprint. Discussion started: 11 November 2026
© Author(s) 2026. CC BY 4.0 License.



Aerosol Reanalysis, 1980 Onward. Part I: System Description and Data Assimilation Evaluation, J. Clim., 30, 6823–6850, https://doi.org/10.1175/JCLI-D-16-0609.1, 2017.

Saxena, P., Hudischewskyj, A. B., Seigneur, C., and Seinfeld, J. H.: A comparative study of equilibrium approaches to the chemical characterization of secondary aerosols, Atmos. Environ., 20, 1471–1483, https://doi.org/10.1016/0004-6981(86)90019-3, 1986.

Seinfeld, J. H. and Pandis, S. N.: Atmospheric Chemistry and Physics: From Air Pollution to Climate Change, 3rd Edn., John Wiley & Sons, Hoboken, NJ, USA, https://www.wiley.com/en-fr/shop/general-chemistry/atmospheric-chemistry-and-physics-from-air-pollution-to-climate-change-3rd-edition-p-9781118947401, 2016.

Shah, V., Jacob, D. J., Moch, J. M., Wang, X., and Zhai, S.: Global modeling of cloud water acidity, precipitation acidity, and acid inputs to ecosystems, Atmos. Chem. Phys., 20, 12223–12245, https://doi.org/10.5194/acp-20-12223-2020, 2020.

Strahan, S. E., Duncan, B. N., and Hoor, P.: Observationally derived transport diagnostics for the lowermost stratosphere and their application to the GMI chemistry and transport model, Atmos. Chem. Phys., 7, 2435–2445, https://doi.org/10.5194/acp-7-2435-2007, 2007.

Strode, S. A., Ziemke, J. R., Oman, L. D., Lamsal, L. N., Olsen, M. A., and Liu, J.: Global changes in the diurnal cycle of surface ozone, Atmos. Environ., 199, 323–333, https://doi.org/10.1016/j.atmosenv.2018.11.028, 2019.

Tie, X., Madronich, S., Walters, S., Edwards, D. P., Ginoux, P., Mahowald, N., Zhang, R., Lou, C., and Brasseur, G.: Assessment of the global impact of aerosols on tropospheric oxidants, J. Geophys. Res., 110, D03204, https://doi.org/10.1029/2004JD005359, 2005.

Valin, L. C., Russell, A. R., Hudman, R. C., and Cohen, R. C.: Effects of model resolution on the interpretation of satellite NO2 observations, Atmos. Chem. Phys., 11, 11647–11655, https://doi.org/10.5194/acp-11-11647-2011, 2011.

Zhang, K., O'Donnell, D., Kazil, J., Stier, P., Kinne, S., Lohmann, U., Ferrachat, S., Croft, B., Quaas, J., Wan, H., Rast, S., and Feichter, J.: The global aerosol-climate model ECHAM-HAM, version 2: sensitivity to improvements in process representations, Atmos. Chem. Phys., 12, 8911–8949, https://doi.org/10.5194/acp-12-8911-2012, 2012.

Zhang, W., Zhang, X., and Wang, H.: The role of aerosol-radiation interaction in the meteorology prediction at the weather scale in the numerical weather prediction model, Geophys. Res. Lett., 49, e2021GL097026, https://doi.org/10.1029/2021GL097026, 2022.

Zheng, B., Zhang, Q., Zhang, Y., He, K. B., Wang, K., Zheng, G. J., Duan, F. K., Ma, Y. L., and Kimoto, T.: Heterogeneous chemistry: a mechanism missing in current models to explain secondary aerosol formation during the January 2013 haze episode in North China, Atmos. Chem. Phys., 15, 2031–2049, https://doi.org/10.5194/acp-15-2031-2015, 2015.